Electrical and optical properties of mixed phase Tungsten Trioxide films grown by Laser Pyrolysis

M. Govender[1, 2*], B. W. Mwakikunga[1+], A. G. J. Machatine[2] and H. W. Kunert[2]

[1] National Centre for Nano-structured Materials, CSIR, P. O. Box 395, Pretoria, 0001, South Africa
[2] School of Physics, University of Pretoria, Pretoria, 0002, South Africa

Keywords laser pyrolysis, tungsten trioxide, nanorods, FIB-SEM, gas sensors

Laser pyrolysis is a synthesis method used to produce thin films and nanomaterials of high quality and purity, by intersecting a laser beam with a chemical precursor. We have chosen laser pyrolysis to synthesize tungsten trioxide starting with tungsten ethoxide precursor. The film had a thickness that varied from 205 nm to 1 μm. X-ray diffraction and Raman spectroscopy confirmed the presence of a mixture of hexagonal and tetragonal phase WO_3 in the synthesized film, and it was clear that annealing greatly influenced the phases and types of structures formed. I-V curves of the films showed n-type semiconducting behaviour, but the mixed phase appeared to cause a similar behaviour of dopants in a semiconductor. The refractive index decreased with increasing wavelength and gave values of up to 21 at low wavelengths. The average optical band gap was found to 3.6 eV from UV/Vis spectroscopy. Scanning Electron Microscopy (SEM) showed a mixture of nano- and microstructures and shapes formed after annealing. One of the grown nanostructures was nanorods, this isolated using FIB for possible applications such as an active sensing medium in gas sensors.

1 Introduction Tungsten trioxide (WO_3) is an n-type semiconducting metal oxide with a wide band gap that exhibit superior electronic and optical properties [1-7]. At room temperature, WO_3 usually exists as a mixture of monoclinic (γ) and triclinic (δ) crystal phase structure, and undergoes phase changes to higher symmetries upon heating [8-12]. WO_3 has commonly been studied for its electro-chromic, gaso-chromic and photo-chromic properties. In recent years, it has been studied for its sensing properties, making it about the fifth most researched metal oxide for this purpose [13].

More focus is put into single crystalline one-dimensional nanostructures of WO_3 such as nanowires because the properties were found to be well tailored for applications such as gas-sensing [14]. The unique properties have been speculated to arise from the anisotropic geometry, large surface-to-volume ratio, and carrier photon/phonon confinement in two dimensions (1-D system) [15]. The synthesis of good quality nanostructures thus becomes imperative and much attention is directed towards controlled synthesis and characterization of nanostructures. It is still challenging to rationally fabricate nanostructures with precisely controlled and tuneable chemical composition, size, structure, morphology and dopants. Therefore, much opportunity exists to try different synthesis techniques depending on the application of the product materials. Here we concern with laser pyrolysis to synthesize WO_3 nanostructures because this technique does not allow the reactants to make contact with any side-walls, and so the products are of high purity and quality [16-18]. It is also shown here how individual nanostructures are isolated for possible sensing applications.

2 Experimental The laser pyrolysis experimental setup was discussed in detail in [19], and only an overview will be presented here. The laser pyrolysis method is carried out inside a stainless steel chamber (see Fig. 1 (a)) at atmospheric pressure. A wavelength tunable continuous wave (CW) CO_2 laser was used in the experiments (Edinburgh Instruments, PL6) and the beam was focused into the reaction chamber. The chosen laser wavelength was 10.16 μm and the measured power density was found to be 51.2 W/cm^2.

The synthesis of tungsten trioxide commenced by mixing 0.1 g of greyish-blue anhydrous tungsten hexachloride WCl_6 (Aldrich 99.9%) powder in 100 mL of absolute ethanol C_2H_5OH (Aldrich 99.9%) to give a tungsten ethoxide $W(OC_2H_5)_6$ starting precursor. The liquid precursor was decanted into an aerosol generator (Micro Mist, model EN) which was attached to the laser pyrolysis system via a multiflow nozzle that allows argon gas to pass through it and carry a stream of very fine precursor droplets (~5 μm droplet diameter according to the manufacturer) into the laser beam. Acetylene (C_2H_2) sensitizer gas and argon encasing gas flowed adjacent to the precursor, guiding it towards a glass substrate as depicted in Fig. 1 (b). The gas flow rates are chosen such that the ablated precursor collects on the

substrate after interacting with the laser. The temperature of the interaction zone of the laser and precursor were considered elsewhere [20] and found to be approximately 127°C. The sample was annealed for 17 hours at 500°C under argon atmosphere [21].

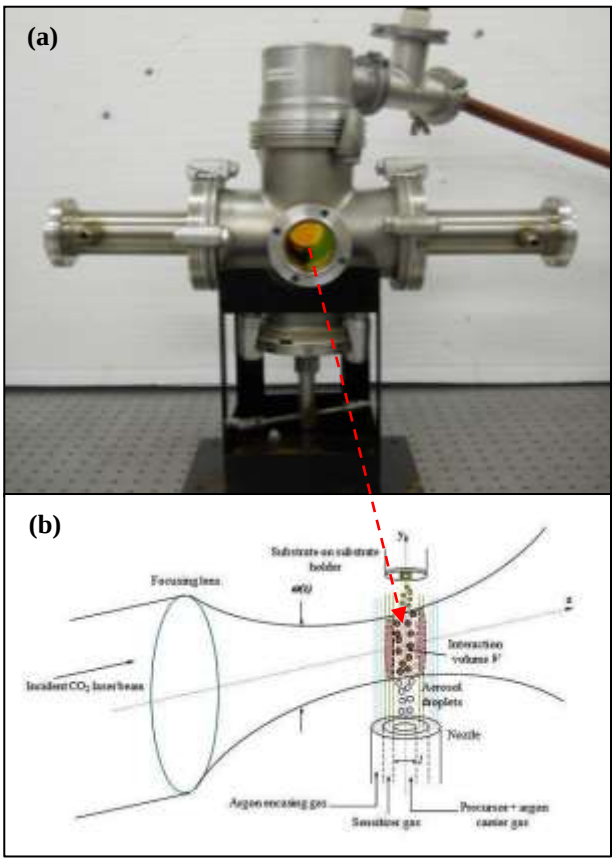

Figure 1 (a) The Laser Pyrolysis chamber and (b) a schematic of the inside of the chamber during synthesis.

Morphology studies were carried out using a Carl Zeiss SMT Auriga™ Scanning Electron Microscopy (SEM) microscope. The Focused Ion Beam (FIB) system used was a Crossbeam® FIB Workstation with Gemini® FESEM Column and worked in tandem with the SEM system. Raman spectroscopy was carried out using a Horiba Jobin-Yvon HR800UV Raman Spectrograph with a wavelength of 514.5 nm from an argon ion laser set at a laser power of ~1 mW at the sample. X-ray diffraction (XRD) was carried out using a Philips Xpert powder diffractometer at a wavelength of 154.184 pm. UV/Vis spectroscopy was carried out using a PerkinElmer Lamda 750S spectrometer in the wavelength range 190-2500 nm, and ellipsometry was carried out on the film using a J. A. Woollam Co. Inc. XLS-100 ellipsometer. I-V curves were taken using a two-point probe (1 mm spacing between probes) system connected to a Keithley 4200 Semiconducting Characterization System.

2 Results and Discussion

2.1 Vibrational and structural analysis Raman and XRD analysis of tungsten trioxide have been reported numerous times [22-26], and despite the simple stoichiometry, the structure is very complex [27-29]. Raman spectroscopy was done on two areas of the sample as denoted by spot 1 and spot 2 of the Raman image shown in the inset of Figure 2. The spectra from either spot had different Raman shifts, indicating the possibility of mixed phases. This could be due to the Gaussian intensity profile of the laser used in the synthesis [18]. There is also a mixture of several shaped nano- and microstructures as seen in the SEM micrographs of Figure ***5***.

The most intense peak in our Raman spectrum shown in Figure 2 of Spot 2 had a shoulder. This peak was deconvoluted into two peaks centred at 775 cm^{-1} and 816 cm^{-1}. ElBatal [25] observed Raman shifts at 333 cm^{-1}, 775 cm^{-1} and 945 cm^{-1} from 10% WO_3 melted together with glass at 1100°C. This combination of peaks is similar to that found in spot 2 of Figure 2 of our synthesized and annealed sample and these peaks arise from a combination of WO_6 groups and the glass. Daniel et al [22] and Breedon et al [26] reported on Raman shifts at 150 cm^{-1}, 165 cm^{-1}, 695 cm^{-1} and 816 cm^{-1} after annealing their samples on glass above 500°C. These peaks were assigned to hexagonal phase WO_3, and according to Gerand et al [30] hexagonal phase WO_3 can be easily obtained by annealing $WO_3.1/3\ H_2O$. According to the peaks at 150 cm^{-1} and 332 cm^{-1}, this strongly suggests the presence of hydrated WO_3 which could have led to the formation of the hexagonal phase WO_3 [31-35]. Analysing spot 1, the peaks at 110 cm^{-1} and 152 cm^{-1} suggest a WO_3 hydrate [22]. The combination of peaks at 704 cm-1 and 798 cm-1 are indicative of tetragonal phase WO_3 [36]. Therefore, spot 1 which appears luminescent when imaged is assigned to tetragonal phase WO_3 and spot 2 which appears has darker material is assigned to hexagonal phase WO_3. Both spots also contain hydrated phases of WO_3.

The XRD diffractogram in Figure 3 was compared to [26, 37-39] and indicates peaks of hydrated, hexagonal phase WO_3, tetragonal phase WO_3 and sodium tungstate. It is noted here that to get an idea of the crystallite size in our sample to correlate with SEM micrographs, Scherrer's formula [40-41] was applied to the peaks in our diffractogram. It was found that the crystallite size varied between 0.47 nm-0.76 nm. Our XRD diffractogram was also compared against the ICCD database and was found to match best with sodium tungstate compound (PDF number 01-080-2471). The sodium tungstate phase was confirmed by the weak Raman shift at 915 cm^{-1} [26] for spot 2 in Figure 2.

It is speculated that the aerosol precursor encounters varying intensities upon entering the laser beam used in laser pyrolysis, which causes different phases, shapes and stoichiometries of WO_3 to form. Furthermore, the influence of glass with its impurities and annealing above

400°C [42-43] appear to significantly influence the vibrational modes of WO_3 as evidenced in the literature.

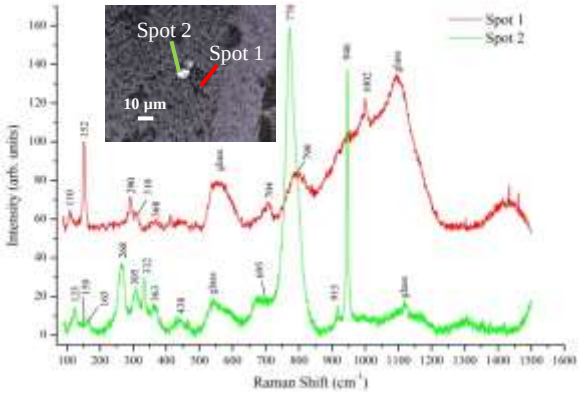

Figure 2 The Raman spectrum showing two spots of different phases and the optical image in the inset shows the variation in the appearance of the material.

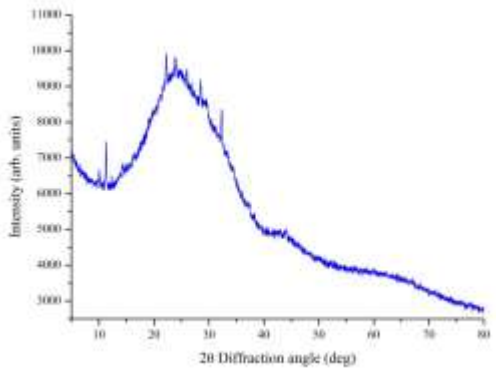

Figure 3 The XRD diffractogram of laser pyrolysis grown film on glass that shows characteristic peaks of sodium tungstate, as well as hexagonal and tetragonal phase WO_3.

2.2 Optical properties The refractive index of the film depends primarily on the deposition and annealing temperature. The thickness of the laser pyrolysis grown film and the effective refractive index was calculated using ellipsometry using the Cauchy model. It should be noted that the laser pyrolysis did not give a uniform film, but instead a thin film at the centre surrounded by a thicker ring of film. Therefore, the thickness given by the ellipsometer is mainly from the centre and thinnest part of the film, which was found to be 205.02±10 nm with a large MSE value of 27. The raw experimental data with the theoretical fit is shown in Figure 4. The refractive index is very high for smaller wavelengths and decreases gradually to very low refractive index for longer wavelengths as shown in Figure 5. This large refractive index is not usually seen for samples annealed at 500°C [44] and this could result from the contribution of the mixture of phases.

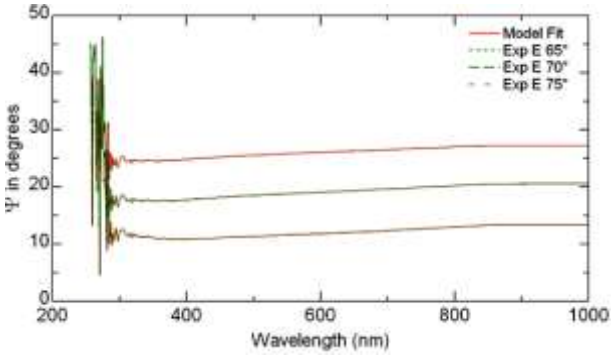

Figure 4 Spectral ellipsometric Ψ data at 65°, 70° and 75° angle of incidence of the laser pyrolysis synthesized mixed phase WO_3 film.

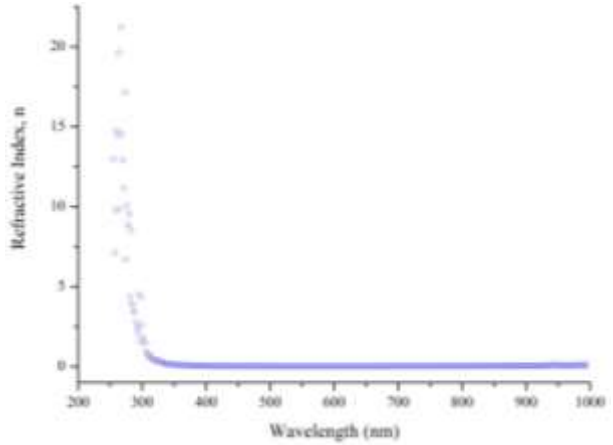

Figure 5 Effective refractive index vs. light wavelength for the laser pyrolysis synthesized mixed phase WO_3 film.

Optical transmittance (%T) was carried out on the film and shows a very high transparency in the spectral region and transmits less light below the spectral region. Below this spectral region, the logarithm of the absorption coefficient α vs. photon energy $h\nu$ shows a linear dependence. Plotting the dependence $(\alpha h\nu)^{1/2}$ vs. $h\nu$, the optical band gap is determined by extrapolating to zero absorption [44]. Since our sample did not have uniform thickness, we took the thickness given from ellipsometry as 205.02±10 nm and 1000±25 nm from cross-sectioning the sample. Cross-sectioning was done by using FIB to cut into the film and under SEM, the film thickness was measured. The optical band gap was found to be 3.74±0.05 eV for a 205 nm thick film and 3.69±0.03 eV for a 1000 nm thick film from Figure 6. The average band gap is much higher than the 3.25 eV quoted in literature for WO_3 annealed at 500°C [45]. The interaction of hexagonal and tetragonal phase WO_3 could be the cause of this difference.

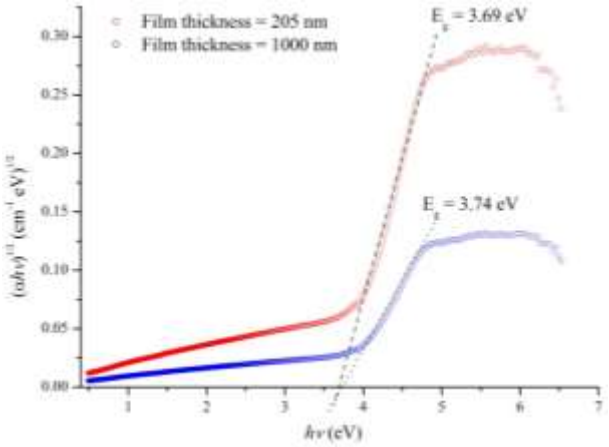

Figure 6 $(\alpha h\nu)^{1/2}$ vs. $h\nu$ plots for the laser pyrolysis synthesized mixed phase WO_3 film for the thinnest and thickest part of the film. Linear fits of the absorption data indicate the indirect band gap of WO_3.

2.3 Electrical properties Using a two-probe setup, a sweeping voltage between -5 V and 5 V was passed through the film while the other probe measured current. The sample was measured at liquid nitrogen temperature by pouring liquid nitrogen on the film. The sample was also measured at 300°C by placing the film on a hot-plate. From Figure 7 of the I-V curve, the film exhibits n-type semiconducting behavior by decreasing in resistance with increasing temperature [46]. The film reaches threshold current at 2.8 V at liquid nitrogen temperature, and 2.4 V at room temperature. The film exhibits metallic behavior at higher temperatures by reaching threshold voltage at 0.2 V as the gap between the conduction and valence band almost overlap. The shape of the curves at room and liquid nitrogen temperature are similar to that of doped metal oxide semiconductors [47]. It is probable that the mixed phases influences the electron carrier properties in a way similar to how dopants influence the carrier properties in a metal oxide.

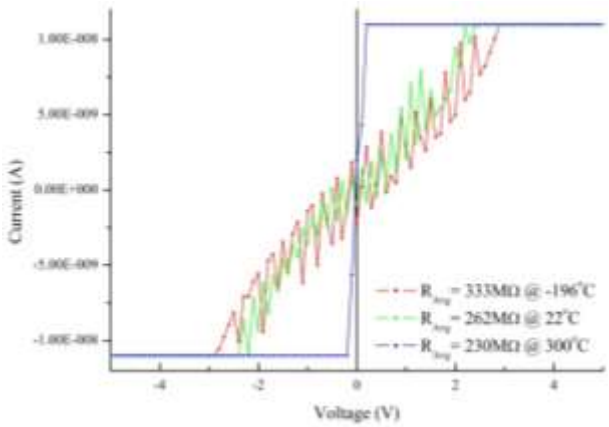

Figure 7 I-V curves of the film taken at liquid nitrogen temperature, room temperature and 300°C.

3 Applications Using Focused Ion Beam-Scanning Electron Microscopy (FIB-SEM), platinum (Pt) contacts can be made on either side of the nanorod so that an electric circuit is produced. The nanorod can now be used as an active sensing-medium for example, making it possible to perform gas sensing. The electronic properties can be measured through the wire via the Pt contacts when a gas is adsorbed on the nanorod surface. Fig. 5 (a-e) shows the progression from identifying a nanorod on the sample surface with SEM to making Pt-contacts with FIB. The next step will be to connect the Pt contacts to a microcircuit and do I-V curve measurements from the single nanostructure and compare it to the bulk [48].

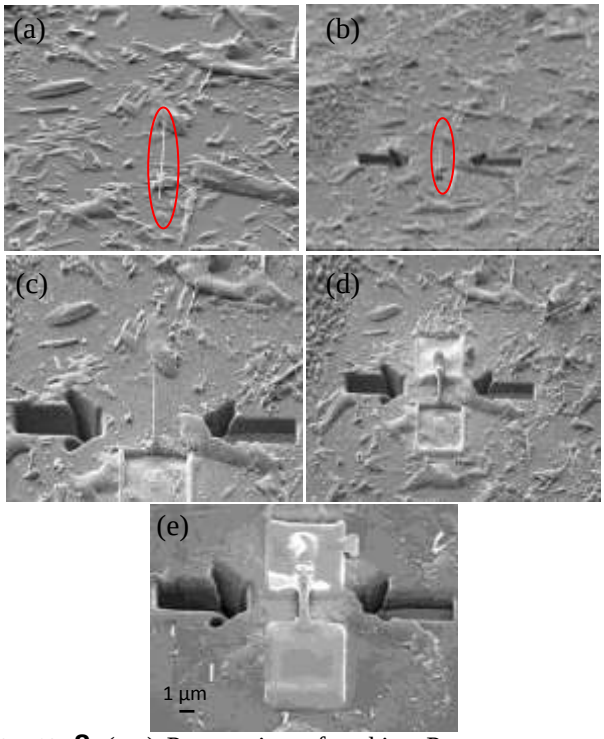

Figure 8 (a-e) Progression of making Pt-contacts on a WO_3 nanorod with FIB and SEM imaging.

Acknowledgements The CSIR National Laser Centre for the equipment used in this study.

References

[1] J. L. Solis, S. Saukko, L. B. Kish, C. G. Granqvist, and V. Lantto, Sens. Actuators B **77**, 316-321 (2001)
[2] S. C. Moulzolf, S-an Ding, and R. J. Lad, Sens. Actuators B **77**, 375-382 (2001)
[3] K. Aguir, C. Lemire, and D. B. B. Lollman, Sens. Actuators B **84**, 1-5 (2002)
[4] Y. B. Li, Y. Bando, D. Goldberg, and K. Kurashima, Chemical Physical Letters **367**, 214-218 (2003)

[5] L. G. Teoh, Y. M. Hon, J. Shieh, W. H. Lai, and M. H. Hon, Sens. Actuators B **96**, 219-225 (2003)
[6] X. –L. Li, T. –J. Lou, X. –M. Sun, and Y. –D. Li, Inorg. Chem. **43**, 5442-5449 (2004)
[7] K. J. Lethy, S. Potdar, V. P. M. Pillai, and V. Ganesan, J. Phys. D: Appl. Phys. **42**, 095412 (2009)
[8] E. Salje, Acta. Cryst. A **31**, 360 (1975)
[9] E. Salje, and K. Viswanathan, Acta. Cryst. A **31**, 356 (1975)
[10] K. R. Locherer, I. P. Swainson, and E. K. H. Salje, J. Phys.: Condens. Matter **11**, 6737-6756 (1999)
[11] M. Boulova, N. Rosman, P. Bouvier, and G. Lucazeau, J. Phys.: Condens. Matter **14**, 5849-5863 (2002)
[12] Y. Fujioka, J. Frantti, and V. Lantto, Integrated Ferroelectrics **123**, 81-86 (2011)
[13] K. J. Choi, and H. W. Jang, Sensors **10**, 4083-4099 (2010)
[14] M. M. Arafat, B. Dinan, S. A. Akbar, and A. S. M. A. Haseeb, Sensors **12**, 7207-7258 (2012)
[15] B. W. Mwakikunga, E. Sideras-Haddad, A. Forbes, and C. Arendse, Phys. Stat. Sol. (a) **205**, 150-154 (2008)
[16] B. W. Mwakikunga, A. Forbes, E. Sideras-Haddad, and C. Arendse, Nanoscale Res. Lett. **3**, 372 (2008)
[17] L. Shikwambana, M. Govender, B. W. Mwakikunga, E. Sideras-Haddad, and A. Forbes, Advanced Materials Research **227**, 80-83 (2011)
[18] M. Govender, L. Shikwambana, B. W. Mwakikunga, E. Sideras-Haddad, R. M. Erasmus, and A. Forbes, Nanoscale Research Letters **6**, 166 (2011)
[19] B. W. Mwakikunga, A. Forbes, E. Sideras-Haddad, R M Erasmus, G. Katumba, and B. Masina, Int. J. Nanoparticles **1**, 3 (2008)
[20] B. W. Mwakikunga, A. E. Mudau, N. Brink, and C.J. Willers, Appl. Phys B **105**, 451-462 (2011)
[21] B. W. Mwakikunga, E. Sideras-Haddad, M. Witcomb, C. Arendse, and A. Forbes, J. Nanosci. & Nanotechnol **9**, 3286 (2008)
[22] M. F. Daniel, B. Desbat, J. C. Lassegues, B. Gerand, and M. Figlarz, Journal of Solid State Chemistry **67**, 235-247 (1987)
[23] K. Nonaka, A. Takase, and K. Miyakawa, Journal of Materials Science Letters **12**, 274-277 (1993)
[24] D. Y. Lu, J. Chen, H. J. Chen, L. Gong, S. Z. Deng, N. S. Xu, and Y. L. Liu, Appl. Phys. Lett. **90**, 041919 (2007)
[25] F. H. ElBatal, Indian Journal of Pure and Applied Physics **47**, 471-480 (2009)
[26] M. Breedon, P. Spizzirri, M. Taylor, J. du Plessis, D. McCulloch, J. Zu, L. Yu, Z. Hu, C. Rix, W. Wlodarski, and K. Kalamtar-zadeh, Crystal Growth and Design **10**, 430-439 (2010)
[27] P. M. Woodward, A. W. Sleight, and T. Vogt, J. Phys. Chem. Solids **56**, 1305-1315 (1995)
[28] M. Boulova, G. Lucazeau, T. Pagnier, and A. Gaskov, J. Phys. IV Frnace **11** 1057-1062 (2001)
[29] C. J. Howard, V. Luca, and K. S. Knight, J. Phys.: Condens. Matter **14**, 377-387 (2002)
[30] B. Gerand, G. Nowogrocki, J. Guenot, and M. Figlarz, Journal of Solid State Chemistry **29**, 429-434 (1979)
[31] A. Cremonesi, D. Bersani, P. P. Lottici, Y. Djaoued, and P. V. Ashrit, Journal of Non-Crystalline Solids **345-346**, 500-504 (2004)
[32] C. Santato, M. Odziemkowski, M. Ulmann, and J. Augustynski, J. Am. Chem. Soc. **123**, 10639-10649 (2001)
[33] C. Balázsi, L. Wang, E. O. Zayim, I. M. Szilágyi, K. Sedlacková, J. Pfeifer, A. L. Tóth, and P. -I. Gouma, Journal of the European Ceramic Society **28**, 913-917 (2008)
[34] T. Peng, D. Ke, J. Xiao, L. Wang, J. Hu, and L. Zan, Journal of Solid State Chemistry **194**, 250-256 (2012)
[35] H. –F. Pang, X. Xiang, Z. –J. Li, Y. –Q. Fu, and X. –T. Zu, Phys. Status Solidi A **209**, 537-544 (2012)
[36] L. Van. Ngoc, T. C. Vinh, L. Q. Toai, N. D. Thinh, H. T. Dat, T. Tuan, and D. A. Phuong, VNU Journal of Science, Mathematics-Physics **25**, 47-55 (2009)
[37] C. Cantalini, H. T. Sun, M. Faccio, M. Pelino, S. Santucci, L. Lozzi, and M. Passacantando, Sens. Actuators B **31**, 81-87 (1996)
[38] I. Jiménez, J. Arbiol, A. Cornet, and J. R. Morante, IEEE Sensors Journal **2**, 329-336 (2002)
[39] Z. Liu, M. Miyauchi, T. Yamazaki, and Y. Shen, Sens. Actuators B **140**, 514-219 (2009)
[40] S. –H. Wang, T. –C. Chou, and C. –C. Liu, Sens. Actuators B **94**, 343-351 (2003)
[41] G. Singla, K. Singh, and O. P. Panday, Powder Technology **237**, 9-13 (2013)
[42] R. E. Tanner, A. Szekeres, D. Gogova, and K. Gesheva, Applied Surface Science **218**, 162-168 (2003)
[43] Y. Djaoued, p. V. Ashrit, S. Badilescu, R. Brünning, Journal of Sol-Gel Science and Technology **28**, 235-244 (2003)
[44] D. Gogova, K. Gesheva, A. Szekeres, and M. Sendova-Vassileva, Phys. Stat. Sol. (a) **176**, 969 (1999)
[45] S. K. Gullapalli, R. S. Vemuri, and C. V. Ramana, Applied Physics Letters **96**, 171903 (2003)
[46] H. Zheng, J. Z. Ou, M. S. Strano, R. B. Kaner, A. Mitchell, and K. Kalantar-zadeh, Adv. Funct. Mater. **21**, 2175-2196 (2011)
[47] T. Zhai, X. Fang, M. Liao, X. Xu, H. Zeng, B. Yoshio, and D. Golberg, Sensors **9**, 6504-6529 (2009)
[48] M. Gillet, R. Delamare, and E. Gillet, Eur. Phys. J. D **34**, 291-294 (2005)